Remote Sensing of the Mean Annual Surface Temperature and Surface Frost Number for Mapping Permafrost in China

Authors: Ran, Youhua, Li, Xin, Jin, Rui, and Guo, Jianwen

Source: Arctic, Antarctic, and Alpine Research, 47(2) : 255-265

Published By: Institute of Arctic and Alpine Research (INSTAAR), University of Colorado

URL: https://doi.org/10.1657/AAAR00C-13-306

Arctic, Antarctic, and Alpine Research, Vol. 47, No. 2, 2015, pp. 255–265

Remote sensing of the mean annual surface temperature and surface frost number for mapping permafrost in China

Youhua Ran[1]
Xin Li[1,2,3]
Rui Jin[1] *and*
Jianwen Guo[1]

[1]Key Laboratory of Remote Sensing of Gansu Province, Cold and Arid Regions Environmental and Engineering Research Institute, Chinese Academy of Sciences, 320 West Donggang Road, Lanzhou 730000, China
[2]Chinese Academy of Sciences Center for Excellence in Tibetan Plateau Earth Sciences, Beijing 100101, China
[3]Corresponding author:
lixin@lzb.ac.cn

Abstract

The use of satellite-infrared sensors to map permafrost distribution is a new research topic. Two important permafrost indices, the mean annual surface temperature (MAST) and the surface frost number (SFN), are estimated using MODIS Aqua/Terra LST products based on a pragmatic scheme proposed in this study. The advantage of this approach is that it allows the full use of every value at any time and at any pixel of MODIS LST products. This scheme is simple, easy to implement, and independent of other observations. The accuracy of the method depends only on the accuracy of the MODIS LST products. Eight years of data sets from 2003 to 2010 were generated using this scheme to reflect the spatial distribution of permafrost and the surface thermal state. A comparison between the southern/lower limit of permafrost and results from the 8-year average MAST and SFN show that the 0 °C MAST isotherm and 0.5 contour of SFN agree well with the identified southern/lower limits of permafrost in China.

DOI: http://dx.doi.org/10.1657/AAAR00C-13-306

Introduction

Permafrost is one of the most important cryospheric components and is sensitive to climate warming and human activity (Li et al., 1996; Jin et al., 2000; Wu et al., 2002; Haeberli and Hohmann, 2008; Li et al., 2008). The areal extent of permafrost in China ranks the third in the world and is the largest in terms of elevational permafrost areas, which are sensitive to climate change. Significant permafrost degradation has occurred and continues to occur in most permafrost regions in China, resulting in increased environmental fragility and related hazards (Wang et al., 2000; Wu and Liu, 2004; Jin et al., 2007, 2009, 2011). All of these factors emphasize the importance of permafrost mapping in China.

Mean annual ground temperature (MAGT), which is usually measured at depths of 10–25 m (the depth of zero amplitude for fluctuations in ground temperatures), is the most direct and reliable indicator of the occurrence of permafrost, but it is expensive and only available at local scales. In China, numerous maps have been compiled to determine the distribution and thermal state of permafrost based on near-surface air temperatures (LIGG/CAS, 1988; Li and Cheng, 1996; Zhou et al., 2000; CAREERI/CAS, 2006; Ran et al., 2012a). However, many investigators suggest that air temperature is not an optimal predictor of permafrost distribution because of the very large insulation effects of the air layer. Instead, with the success of thermal-infrared remote sensing technology, the land surface temperature (LST) provides a more direct indicator for the occurrence of permafrost and should be used instead (Nelson and Outcalt, 1987; Hachem et al., 2009; Wang et al., 2011).

Satellite image data have been successfully used to retrieve the LST since the advent of the Advanced Very High Resolution Radiometer (AVHRR) instrument on board the National Oceanic and Atmospheric Administration (NOAA) series of satellites since the early 1970s and the Moderate Resolution Imaging Spectroradiometer (MODIS) instrument, which was launched in 2000 as a payload on the Terra satellite. In 2002, a second MODIS instrument was launched on the Aqua satellite. MODIS improves the performance of the AVHRR by providing a higher spatial resolution and greater spectral resolution. The polar-orbiting MODIS sensors produce daily LST maps with global coverage. A significant number of validations around the world have shown that the accuracy of the MODIS LST product is approximately 1 K in most cases (Wan, 2008). However, the remote sensing observation is instantaneous. The satellite thermal infrared channels are susceptible to the influence of clouds, although they are highly accurate for LST retrieval using thermal infrared channels. Therefore, methods for calculating the quantitative criteria for the mapping of permafrost, such as the mean annual surface temperature (MAST) and surface frost number (SFN), are important.

Based on remote sensing LST observations, numerous studies have attempted to estimate the mean LST. A simplified method was proposed by Jin (2000) that includes the following two steps: the neighboring-pixel approach and surface air temperature adjustment. The scheme has a clear theoretical basis, but poses several problems; for example, many parameters are difficult to achieve, and the spatial coverage is inadequate. Langer et al. (2010) and Westermann et al. (2011) examined the spatial and temporal variability of summer LSTs using a ground-based high resolution thermal imaging system at a polygonal tundra site in northern Siberia, Russia, and a High Arctic tundra in Svalbard, Norway. Langer et al. (2010) noted that cloudy conditions might lead to biased weekly temperature averages, which was inferred from the MODIS LST data, and recommended a solution to improve the accuracy of average LST values by combining cloud cover information with a gap-filling procedure. Westermann et al. (2011) concluded that a reliable gap-filling procedure to moderate the effect of prolonged cloudy periods would be of significant value for future LST-based permafrost monitoring schemes. Hachem et al. (2009, 2012) proposed a more practical method for estimating the MAST. This

1523-0430/04 $7.00

method involves fitting a sinusoidal model over the daily LST from MODIS readings to reproduce the seasonal thermal variations near the ground for each 1 × 1 km pixel. However, limited research has been conducted to estimate the MAST and SFN using MODIS LST products in China.

In this study, we propose a pragmatic scheme for estimating the MAST and SFN using MODIS Aqua/Terra LST products, which provide four daily LST observations. Eight years of data sets from 2003 to 2010 are generated using this scheme to determine the spatial distribution of permafrost and the surface thermal state. An extensive validation and case application show the potential of the MODIS MAST and SFN products. However, certain key problems should be addressed so that the permafrost distribution may be more accurately mapped.

Methodology

ASSUMPTION

The assumption that the arithmetic average of the maximum and minimum LSTs can represent the daily mean LST has been well established (Liu et al., 2006; Kogan et al., 2010; Ran et al., 2012b). Thus, MODIS Terra/Aqua daytime and nighttime LST products (MOD11C1 and MYD11C1 Version 041) with a 0.05º ´ 0.05º spatial resolution (about 5.6 km) were acquired from the U.S. National Aeronautics and Space Administration (NASA) Distributed Active Archive Center (DAAC) and used to estimate the daily mean LST.

IMPLEMENTATION OF THE METHOD

Based on the above assumption and the spatiotemporal correlation of LST, a pragmatic scheme is presented to estimate the MAST and SFN. The workflow of this scheme is shown in Figure 1, and it includes the following five steps:

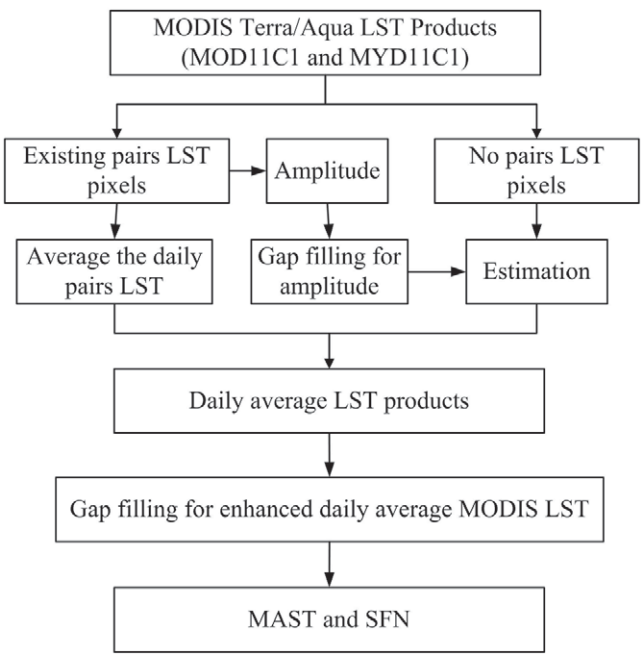

FIGURE 1. The flowchart for estimating the mean annual surface temperature (MAST) using the MODIS Aqua/Terra daytime and nighttime land surface temperature (LST) products. SFN is surface frost number.

Step 1: Select the Daytime and Nighttime LSTs

The mean daily LST for one day is calculated using Equation 1. At least one daytime and one nighttime observation is selected from the Aqua and Terra MODIS sensors.

$$T_{daily} = (T_d + T_n)/2, \tag{1}$$

where, *d* denotes daytime; *n* nighttime; *daily* the mean daily LST, and *T* represents the LST.

Step 2: Identify the LST Amplitude and Interpolate It over the Concerned Region

To estimate the mean daily LST for the pixels without a pair of LST observations, which usually occurs under cloud-cover conditions, the daily LST amplitude is used. First, the amplitude (*D*) is calculated using Equation 2. Then, gap filling is implemented to restore missing amplitude by using a smoothing algorithm that employs a penalized least square regression based on discrete cosine transforms that explicitly utilizes information from the time-series to predict the missing values (Garcia, 2010). The penalized least square regression is a thin-plate spline smoother for a generally one-dimensional data array, it can trade off fidelity to the data versus roughness of the mean function (Wang, et al., 2012). The mathematical details of the algorithm can be found in Garcia (2010). Based on this step, any one observation is sufficient to estimate the mean daily LST. We believe that such observations are stronger than the absence of observations in this process.

$$D = T_d - T_n. \tag{2}$$

Step 3: Calculate the Mean Daily LST for the Pixels without a Pair of LST Observations, Which Usually Occurs under Cloud-Cover Conditions

With known daily LST amplitude, the mean daily LST for the pixels without a LST pair is calculated using Equation 3, as follows:

$$T_{daily'} = \begin{cases} T_{dt} - D_d/2 & t = 1 \text{ or } 3 \\ T_{dt} + D_d/2 & t = 2 \text{ or } 4 \end{cases}, \tag{3}$$

where, *t* represents the time for one day, the values 1 and 3 indicate the daytime LST, the values 2 and 4 indicate the nighttime LST, *d* denotes one day in a certain year, the term *daily* denotes the mean daily LST for the pixels without a LST pair.

Step 4: Fill Gaps for the Enhanced Daily Average MODIS LST

The mean daily LST is expanded spatially as much as possible by steps 2 and 3. For step 4, gap filling is implemented for the enhanced time-series daily average MODIS LST data sets using a same algorithm with restore missing amplitude in step 2. After the above steps were completed, the temporally and spatially continuous daily average LSTs from 1 January 2002 to 31 December 2010 were generated.

Step 5: Production of the MAST and SFN

According to the daily average MODIS LST, the MAST and SFN are produced. In this study, the SFNs (Nelson and Outcalt, 1987) are calculated using Equation 4, as follows:

$$F = \frac{DDF^{1/2}}{DDF^{1/2} + DDT^{1/2}}, \quad (4)$$

where *DDF* and *DDT* are the ground surface freezing and thawing indices, respectively, expressed in degree-days, and *F* is the SFN. The freezing and thawing indices (the degree-day totals above and below 0 °C) are derived from the daily average MODIS LST.

VALIDATION

Temperature-based and radiance-based methods were used to validate the estimated MAST based on the MODIS LST. For the temperature-based method, because the ground-based LST measurement also has strong noise and is ill-matched with the satellite pixels at the spatial dimension, the land surface air temperature is used to evaluate the estimated MODIS MAST. The in situ daily land surface air temperature at six sites (the top six sites in Table 1) in the permafrost regions and the mean annual land surface air temperatures (MAAT) at 724 sites in China are obtained from the Chinese Meteorological Administration (CMA).

Relative to the temperature-based method, the spatial scale of radiance-based LST measurements is more similar to the MODIS pixel, but the available data are very limited. In this study, the radiance-based LSTs from two sites, Arou and Yingke in the eastern Qilian Mountains in Table 1, are used. These two sites are part of establishments of the WATER experiment (Li et al., 2009). At the two radiance-based sites, four components of radiation, including the total solar radiation, reflective short-wave radiation, land surface long-wave radiation, and atmospheric long-wave radiation, were measured. The emissivity values are empirically assigned according to the land cover types and vegetation fraction. Based on these observations, the LST values at these two sites are estimated using Equation 5, as follows:

$$T_s = \left[\frac{F^{\uparrow} - (1-\varepsilon_b) \cdot F^{\downarrow}}{\varepsilon_b \cdot \sigma} \right]^{1/4}, \quad (5)$$

TABLE 1

Descriptions of the six sites in the permafrost region and two radiance-based LST sites.

ID	Name	Location	Elevation (m)	Landscape
1	Wudaoliang	35°13′N, 93°5′E	4612.2	Desert steppe
2	Shiquanhe	32°30′N, 80°5′E	4278.6	Cold desert
3	Amdo	32°21′N, 91°6′E	4800	Alpine meadow
4	Tuotuohe	34°13′N, 92°26′E	4533.1	Alpine meadow
5	Mo'he	52°58′N, 122°31′E	433	Urban
6	Daxinganling	50°24′N, 124°7′E	371.7	Forest
7	Arou	38°03′N, 100°27′E	3033	Alpine meadow
8	Yingke	38°51′N, 100°25′E	1519	Cropland

where T_s is the LST, $F^{\uparrow}$ is the land surface upwelling long-wave radiation, ε_b is the surface broadband emissivity, $F^{\downarrow}$ is the surface atmospheric down-welling long-wave radiation, and σ is the Stefan-Boltzmann's constant (5.67×10^{-8} Wm^{-2} K^{-4}).

Three statistical indexes were used to evaluate the estimated MAST based on the MODIS LST with the surface air temperatures or radiance-based LST observations, which include the Pearson correlation coefficient (*R*), the mean difference (MD), and the standard deviation of the MD (SD). *R* was used as a measure of the degree of association between MODIS LST and in situ temperature measurements (radiance-based LSTs or air temperatures). The MD was used as a measure of the difference between the two sets of data. If the MD is negative, the MODIS-based LST is larger than the radiance-based LST or air temperature. Inversely, positive MD denotes that the MODIS-based LST is lower than the observed temperature. The SD was used to assess the variability of the MD.

Results and Validation

The MAST and SFN derived from the original MODIS LST products from 2003 to 2010 are generated by implementing the method described in the last section. Figure 2 shows the MAST and SFN in 2008. The estimated MAST in China shows the expected latitudinal and elevational gradients. Figure 2 (left) shows the spatial patterns of the MAST distribution in China. The MASTs in northern China and the Qinghai-Tibet Plateau (QTP) are colder than in southern China. The MASTs in the mountainous regions, including the Tianshan, Altai, Qilian, Himalaya, Kunlun, Tanggula, Hengduan, Yin, Changbai, and Da and Xiao Xing'anling Mountains, are colder than in other regions. The SFN patterns are similar to those of MAST and can be found in Figure 2 (right).

EVALUATION OF THE METHOD

The scheme proposed in this study is designed to effectively restore the missing values of the MODIS original LST products in time and space with a minimal loss of accuracy. In this section, the half-hour time resolution radiance-based LST data in 2008 at the Arou and Yingke stations, and the maximum, minimum, and daily average land surface air temperatures in 2008 at the six sites (the top six sites in Table 1) are used to evaluate the effectiveness of this scheme in the temporal dimension. In the spatial dimension, the available daily average air temperatures at the 684 sites are used.

In the temporal dimension, in 2008 there are only 199 days at Arou, and 221 days at Yingke with effective daily average LSTs in step 1. These are expanded to 313 days at Arou, and 323 days at Yingke after step 3. After step 4, all of the missing values are restored. Table 2 provides the accuracy profile through the process from the original MODIS LST to that after the Step 1, 2, and 4. It shows that the accuracy is insignificantly reduced after the final gap-filling in step 4. Step 1 represents the maximum possible accuracy in the scheme. After four steps, the final accuracy is nearly equal to the maximum possible accuracy and may even better it in certain cases. The source of the error in the final LST product is primarily from the original MODIS LST observations, especially the Terra and Aqua daytime LST products. This situation occurs at most of the sites on the QTP, and it is obvious at the Wudaoliang, Amdo, and Tuotuo'he stations on the interior QTP (Table 2). This distinction can be explained by the MODIS cloud detection scheme failing to recognize certain cloud-covered or partially cloud-covered situations. During the summer season, the higher LST is more sensitive to the cloud cover. Overall, the MODIS daily average

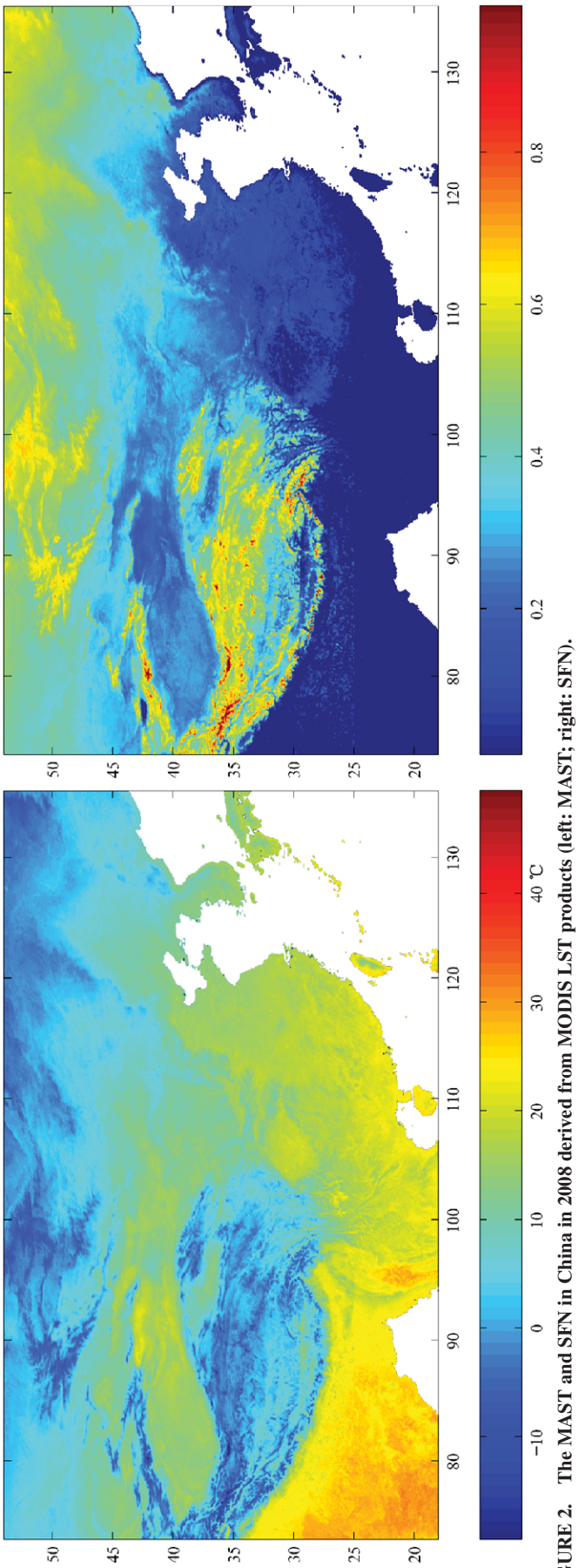

FIGURE 2. The MAST and SFN in China in 2008 derived from MODIS LST products (left: MAST; right: SFN).

LST represents a similar annual cycle to the measurements of surface air temperature or radiance-based LST (Figure 3).

A similar situation occurs for the spatial dimension (Fig. 4). Figure 4 shows the spatial expansion and accuracy change from steps 1 to 4 for the daily average LST on 26 October 2008. The effective pixel number of MODIS LST in step 1 only accounts for 24.75% of the total pixel number, and it is expanded to 51.35% after step 3. After step 4, all of the missing values are restored. The *R* of the MODIS LST for the three steps with the corresponding surface air temperatures are 0.83, 0.79, and 0.86, respectively. The MD and SD are reduced significance also.

This analyses shows that the scheme proposed in this study provides accurate estimations of the MAST from the original MODIS LST products. The method is effective for restoring the missing values of the MODIS instantaneous LST observations, and a space-time continuous daily average LST data set is generated. The accuracy of this data set is nearly equal to the possible accuracy (the maximum accuracy of the MODIS instantaneous LST products) in the temporal and spatial dimensions, and may even be better in certain cases. The source of the error in this data set is primarily from the original MODIS instantaneous LST products, especially for the daytime LST products. In general, the overestimated instantaneous daytime LST leads to an overestimation of the daily average LST.

EVALUATION OF THE RESULTS

The MAATs at the 724 sites in 2008 are used to evaluate the estimated MAST, which is shown in Figure 5. The *R* between the in situ measured MAATs and the estimated MODIS MASTs in 2008 is 0.88, and the MD is –2.98 with a SD of 1.86. The large MD and SD values can be explained by the influence of the surface heterogeneity within the MODIS 5.6 × 5.6 km grid cells, the presence of undetected clouds and the inherent difference between the MODIS skin temperature and the in situ surface air temperature. This strong correlation indicates that the estimated MASTs have a high level of accuracy. However, a systematic bias occurs in the MODIS MAST. In general, the estimated MODIS MASTs are larger than the in situ MAAT measurements by approximately 2.98 °C. This systematic bias has a strong spatial heterogeneity over China. On the QTP, the MD is –3.3 °C, with a SD of 2.79 °C. In Northeast China, it is –1.06 °C, with a SD of 0.72 °C. This spatial heterogeneity is better visualized in Figure 6, which shows the interannual change between the in situ MAAT and MODIS MAST at the six sites in the permafrost regions in China, including the Wudaoliang, Shiquan'he, Amdo, Tuotuo'he, Mo'he, and Daxinganling sites. The MODIS MAST has a consistent trend with the in situ measured MAAT, but it is more consistent in Northeast China than on the QTP.

The systematic bias of the MODIS MAST may partly originate from the overestimated MODIS daytime LSTs in summer, and partly from the inherent difference between MAST and MAAT. Therefore, two issues should be considered in the near future. The first issue is the development of a MODIS cloud detection scheme to effectively recognize the complete or partially cloud-covered situations, or a stronger statistical method to estimate the true LSTs under cloudy conditions. The second issue is to assign threshold of MAST to distinguish permafrost and seasonal frozen ground by comparison of MAST with the MAGT. An indirect application of MAST can be selected to quantify the spatial distribution of the systematic bias, which should aid in translation of the MODIS MAST to MAAT for permafrost mapping using existing threshold

TABLE 2

Mean difference (MD), standard deviation of the MD (SD), and Pearson correlation coefficient (R) between MODIS LST and radiance-based LST (Arou and Yingke) or surface air temperature measurement (other sites).

Site		MOD_day	MOD_night	MYD_day	MYD_night	Step1	Step3	Step4
Wudaoliang	MD	–6.53	0.10	–7.71	2.09	–3.85	–3.82	–3.80
	SD	6.52	3.16	6.80	3.36	3.67	4.14	3.18
	R	0.81	0.94	0.80	0.93	0.92	0.91	0.94
Shiquanhe	MD	–14.15	–0.91	–15.92	2.5	–6.97	–7.14	–6.73
	SD	5.59	3.58	5.50	3.15	3.33	4.24	2.94
	R	0.90	0.94	0.89	0.96	0.96	0.94	0.97
Amdo	MD	–9.43	–0.26	–11.22	2.84	–5.50	–4.91	–4.92
	SD	5.61	3.32	5.16	3.86	3.31	5.11	2.82
	R	0.68	0.95	0.77	0.93	0.93	0.88	0.94
Tuotuo'he	MD	–8.78	–2.02	–9.59	0.14	–5.73	–5.67	–5.70
	SD	6.25	3.08	6.33	3.48	3.47	5.64	3.11
	R	0.77	0.95	0.82	0.94	0.93	0.83	0.94
Mo'he	MD	3.27	–4.39	1.10	–0.49	–1.05	–0.84	–0.65
	SD	4.95	5.07	4.30	4.57	2.95	3.96	3.30
	R	0.98	0.96	0.97	0.97	0.99	0.98	0.98
Daxinganling	MD	0.14	–2.29	–1.39	0.84	–1.47	–1.41	–1.25
	SD	4.33	4.17	4.46	3.97	2.68	3.33	3.18
	R	0.97	0.96	0.96	0.97	0.99	0.98	0.98
Arou	MD	2.02	–3.04	1.52	–1.94	–0.26	0.16	–0.03
	SD	5.50	3.11	4.79	4.84	3.28	3.97	3.85
	R	0.92	0.96	0.93	0.91	0.96	0.94	0.94
Yingke	MD	–9.16	–4.13	–7.96	–2.90	0.27	0.70	0.67
	SD	12.66	4.78	12.82	4.86	6.99	7.36	6.43
	R	0.95	0.98	0.93	0.95	0.95	0.93	0.96

of MAAT. Although the MODIS MAST is not an absolute index for indicating the occurrence of present permafrost, it provides more direct and useful information than the traditional MAAT index and can therefore be used to monitor the permafrost thermal state and its changes.

Comparison with the Permafrost Zone Boundary

Two permafrost maps in China are used to compare the 8-year averages of MAST and SFN at two scales, and they include the modified map of permafrost distribution along the Qinghai-Tibet Highway and Railway, which was developed according to numerous field observations (Tong et al., 1983; Qingbai Wu, unpublished), and an updated map of the distribution of frozen ground in China (Ran et al., 2012a), which was compiled based on the QTP subset of the CAREERI2006 map (CAREERI/CAS, 2006), the Map of Geocryological Regionalization and Classification in China (Zhou et al., 2000), and the new southern limit of permafrost in northeastern China from Jin et al. (2007). According to the MAAT isotherm used in the past (Wang et al., 1979), the 0 °C isotherm of the MAST and the 0.5 contour of SFN are considered to be a southern or lower limit of permafrost in China. Here, we just discuss the 0 °C isotherm of the MAST because it is consistent with the 0.5 contour of SFN.

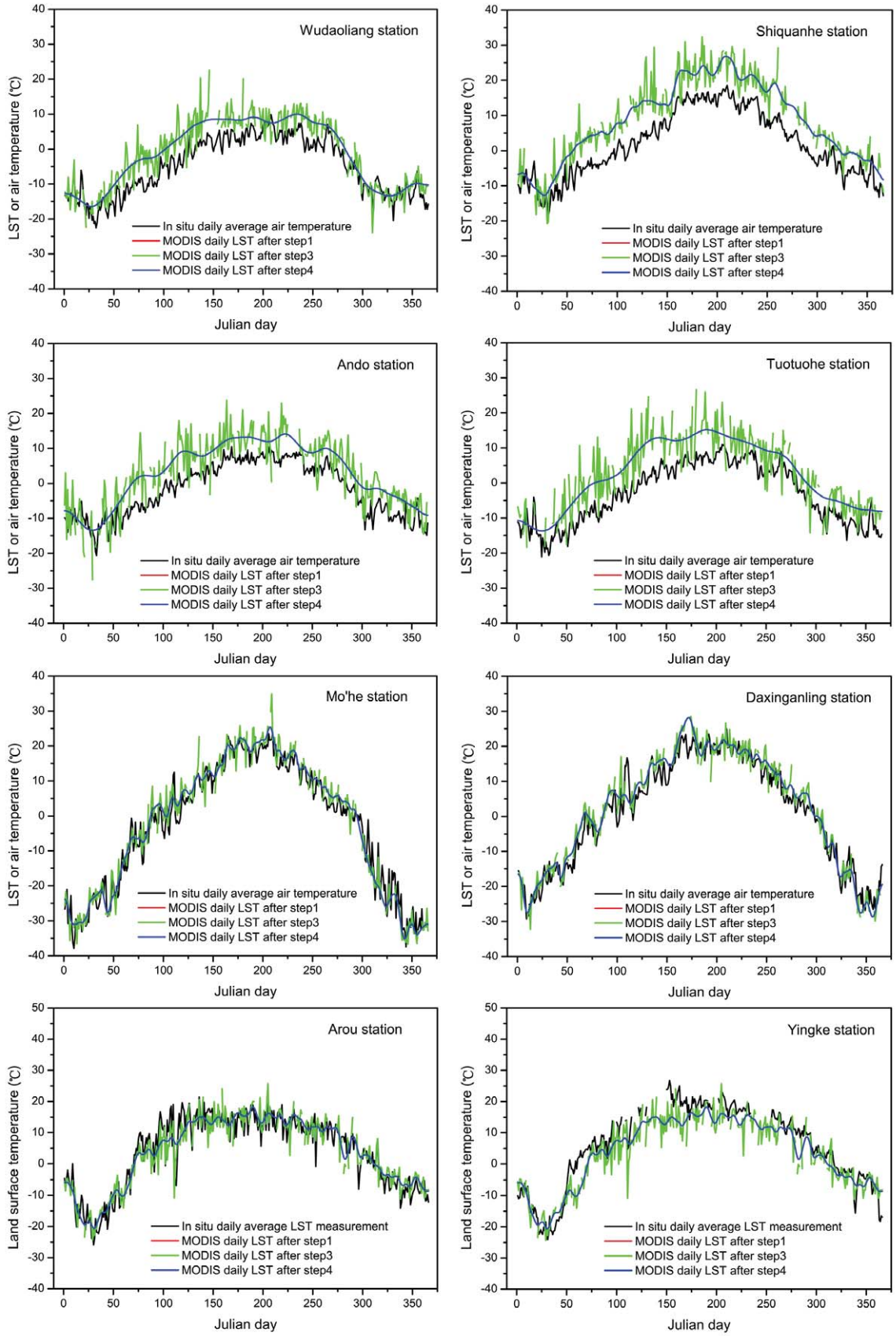

FIGURE 3. The comparison of the estimated daily average LST with in situ daily average air temperature and radiance-based LST measurements in 2008.

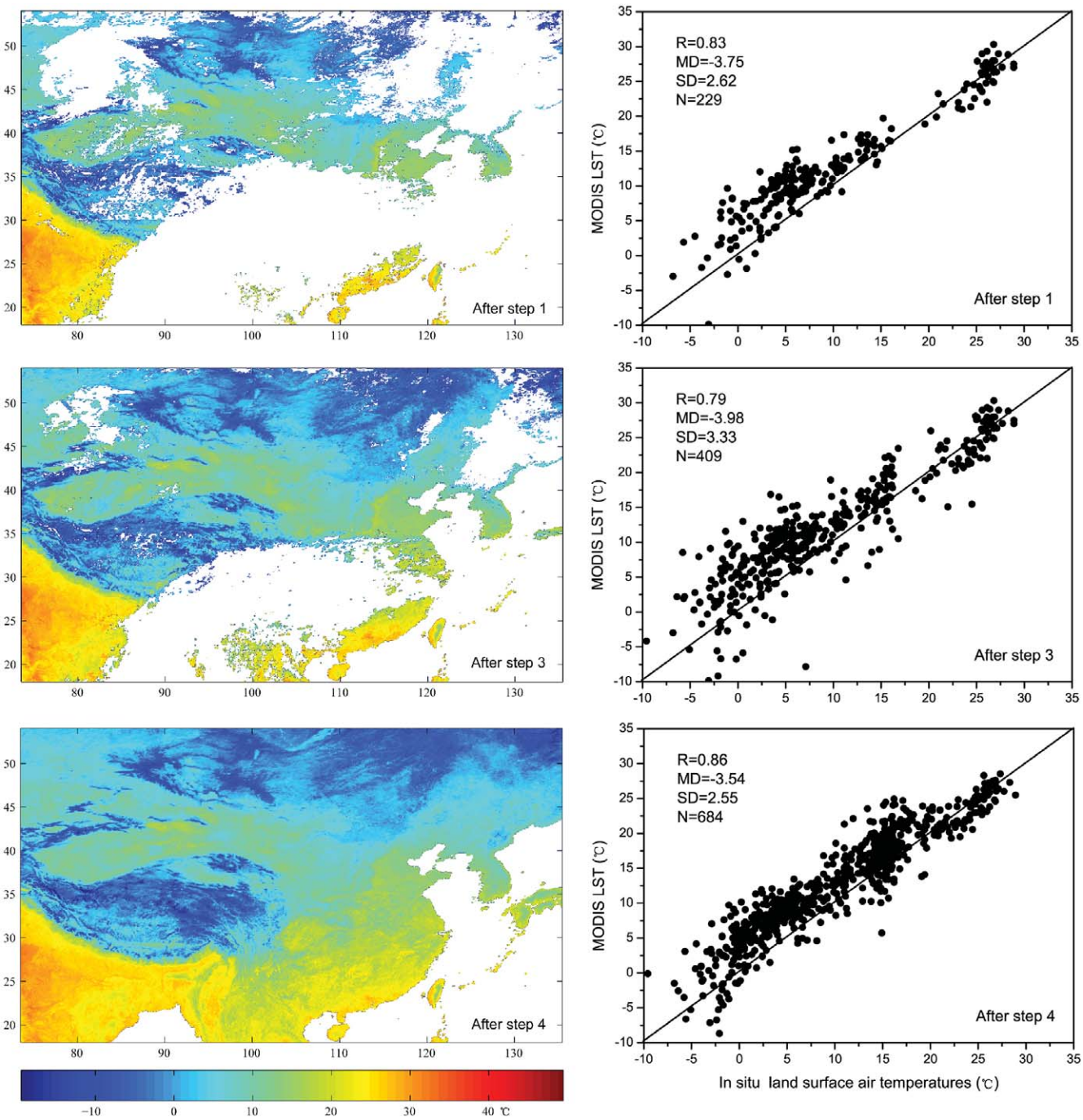

FIGURE 4. The spatial expansion and accuracy change along the method step for the daily average LST on the 300 Julian day in 2008 (26 October 2008).

CONSISTENCY

Overall, the 0 °C MAST isotherms agree reasonably well with the southern limit of permafrost at national and local scales. At the national scale, they agree well with the southern/lower limit of permafrost in the updated map of the frozen ground distribution in China (Fig. 7, part a). The most consistent areas include the alpine permafrost regions in the Qilian, Altai, and Tianshan Mountains, and even in the Changbai and Xing'anling mountains. The possible reason for this consistency is that the strong temperature gradient in mountainous areas makes the pattern of alpine permafrost more easily identified by both MAST and MAAT. The area with a lesser degree of consistency is the high-latitude permafrost regions in Northeast China, and the areas with the least amount of consistency are the permafrost areas on the QTP. The overlapping permafrost area between the 0 °C MAST isotherm and the southern/lower limit of permafrost of updated map of the frozen ground distribution in China exceeds 80%. At a local scale, the 0 °C MAST isotherms agree very well with the southern/lower limit of permafrost derived from the modified map of permafrost distri-

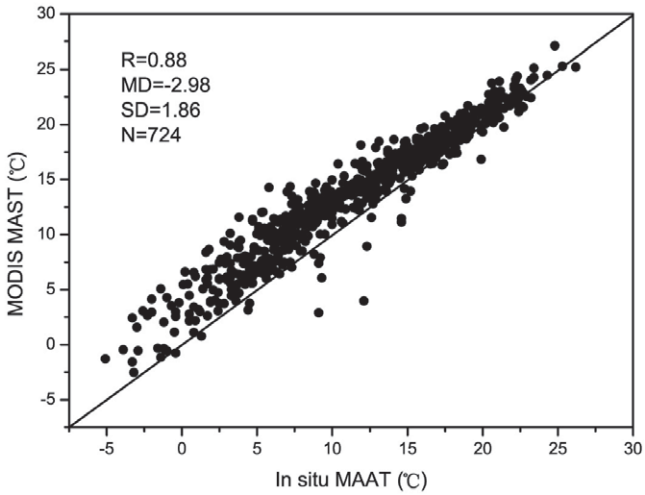

FIGURE 5. The relation of the estimated MODIS MAST and observed mean annual land surface air temperature (MAAT) in 2008.

bution along the Qinghai-Tibetan Highway and Railway. The difference is no greater than 6 km, except in the talik area of Tuotuohe (Fig. 7, part b).

DIFFERENCE

The difference between the 0 °C MAST isotherm and the southern limit of permafrost from the existing permafrost map mainly lies in three regions at a local scale, including southwestern QTP, southeastern QTP, and Northeast China—that is, Regions 2, 3, and 4 in Figure 7, part a, respectively.

In Region 2 (southwestern QTP), the details of the southern limit of permafrost are very different (Fig. 7, part c). This difference is mainly caused by the different resolution between existing permafrost maps and the 0 °C MAST isotherm. The remote sensing data of MAST and SFN show a more detailed permafrost distribution with a higher resolution. Region 2 is located about 600 km east of Shiquan'he town (Fig. 7, part c). The survey data are scarce in this region. Preliminary results from recent surveys indicate that the lower limit of permafrost is more northerly relative to that derived from a published permafrost map (Nan et al., 2013). The 0 °C MAST isotherm is closer to these results. Most parts of Region 3 (southeastern QTP) is covered by glaciers and snow cover. It is not known whether the glaciers are underlain by permafrost, but the 0 °C MAST isotherm lies more southerly than the lower limit of permafrost from the updated map of the frozen ground distribution in China (Fig. 7, part d). The average elevation of the region is relatively low, and no meteorological station is available. The MAAT may be overestimated by the altitude-based surface air temperature interpolation method used in the updated map of the frozen ground distribution in China. In Region 4 (Northeast China), the main difference appears in the east (Fig. 7, part e) where the 0.5-contour of SFN is more southerly than the southern limit of permafrost. In the updated map of the frozen ground in China, the southern limit of permafrost in Northeast China was delineated according to the MAAT isotherms from 33 meteorological stations over the period from 1991 to 2000. However, with the rapid development of urbanization in this region, the environment of many meteorological stations is changed from rural to urban environs. The measured air temperatures could be elevated by the urban "heat island" effect. Therefore, the real southern limit of permafrost could be a little more northerly (Huijun Jin, personal communication).

The difference of the southern/lower limit of permafrost with the 0 °C MAST isotherm and the 0.5-contour of SFN can be described quantitatively by the MAST and SFN along the southern/lower limit of permafrost. Table 3 shows that the lower limits of mountain and plateau permafrost, and the southern limit of latitudinal permafrost agree with the MAST isotherms of 2.95 ± 3.76, 2.14 ± 3.94, and 0.2 ± 1.42 °C respectively. The mean SFN (0.42) is the same in mountain and plateau permafrost zones, equal to with a similar standard deviation. This suggests that the SFN is a more stable indicator than the MAST, because the SFN can suppress the systematic bias of the MODIS MAST. The errors of freezing and thawing indices are offset by the SFN to some extent. The mean

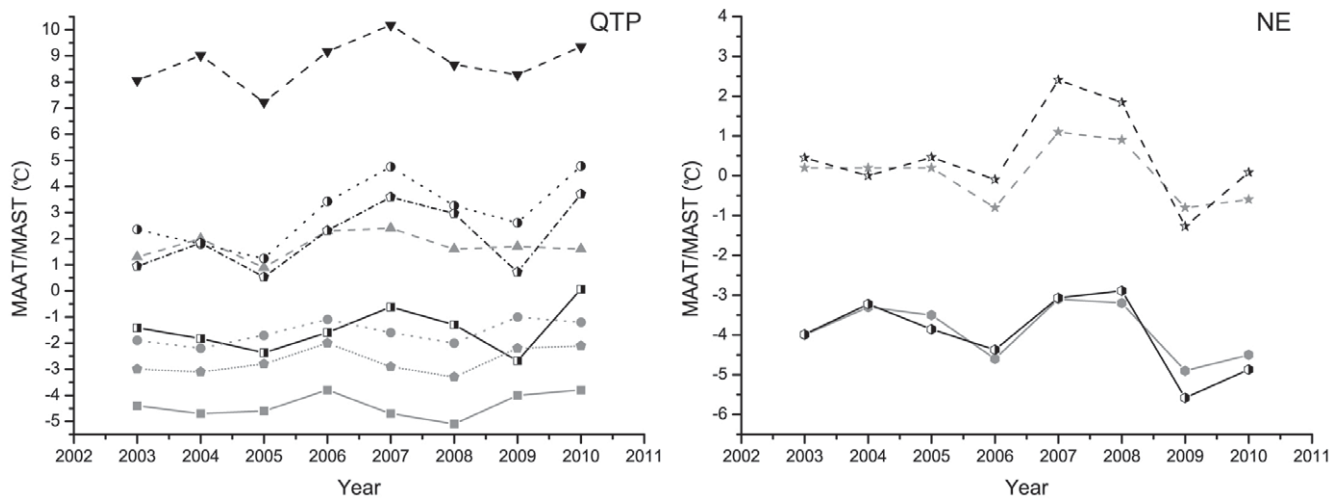

FIGURE 6. Comparison of the annual change between the in situ MAAT and the MODIS MAST. (The gray line is the in situ MAAT, and the black line is the MODIS MAST. Square: Wudaoliang; Triangle: Shiquanhe; Circle: Amdo; Pentagon: Tuotuo'he; Hexagon: Mo'he; Star: Daxinganling).

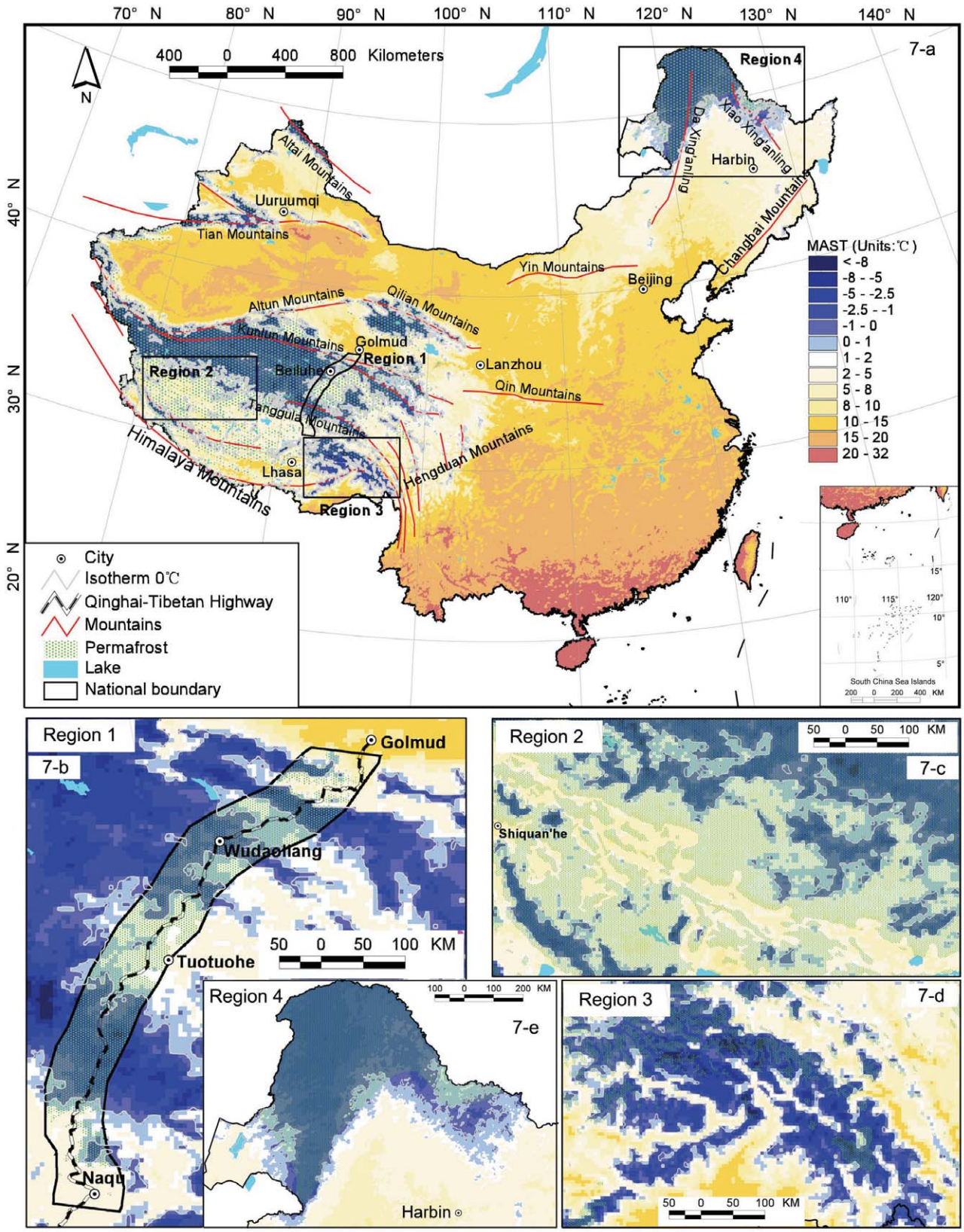

FIGURE 7. Relationship between the 8-year average MAST, SFN, and the southern/lower limits of permafrost in China (a) and in four enlarged areas: (b) along the Qinghai-Tibet engineering corridor, (c) in western QTP, (d) in southeastern QTP, and (e) in northeastern China.

TABLE 3

The mean annual surface temperature (MAST) and surface frost number (SFN) along the southern and lower limits of permafrost in China.

	Mountain permafrost	Plateau permafrost	High-latitude permafrost
MAST	2.95 (SD = 3.76)	2.14 (SD = 3.94)	0.2 (SD = 1.42)
SFN	0.42 (SD = 0.13)	0.42 (SD = 0.15)	0.52 (SD = 0.02)

SFN is 0.52 with a standard deviation of 0.02 in latitudinal permafrost zone in Northeast China. Mountain permafrost is sporadic and discontinuous at the local scale because of strong topographic and microclimatic variability. Therefore, the mountain permafrost is sensitive to spatial location-registration. This characteristic may result in a larger standard deviation in mountain permafrost regions.

In summary, the 0 °C MAST isotherm and 0.5-contour of SFN is consistent with the known southern and lower limits of permafrost in China. These show that the remote sensing MAST and SFN provide a higher resolution for monitoring of the thermal state of permafrost and its changes.

CONCLUSIONS AND PROSPECTS

Mapping permafrost using satellite LST observation is a new research direction. A pragmatic scheme for the estimation of MAST and SFN using the MODIS Aqua/Terra LST products is presented in this paper. The characteristics of this approach include that it allows the full use of every value at any time at any pixel of MODIS LST products, and it is simple, easy to implement, and independent of other observations. Eight years of data sets from 2003 to 2010 were generated using this scheme to denote the spatial distribution of permafrost and the surface thermal state. Extensive validation shows that the scheme proposed in this paper is effective in restore the missing values of MODIS instantaneous LST observations, and in producing a space-time continuous daily average LST data set with a good agreement with ground surface observations. The errors of this data set mainly originate from the original MODIS instantaneous LST products, especially for its daytime LST.

A comparison between the southern/lower limit of permafrost and 8-year average MAST and SFN shows that the 0 °C MAST isotherm and 0.5-contour of SFN agree well with the identified southern/lower limits of permafrost in China. Although the deviation is obvious at local scale, it can be reduced by removal or calibration of the influences of snow and vegetative covers, thermal and physical properties of soils, and other variables. Many methods are available, such as the modified Kudryavtsev's approach (Romanovsky and Osterkamp, 1997; Sazonova and Romanovsky, 2003), and the SFN computational method integrating the effects of snow cover (Nelson and Outcalt, 1987). However, the influences of snow and vegetative covers and thermal and physical properties of soils on the distribution of permafrost are very complex (Zhang, 2005). This method, developed in other permafrost regions such as Siberia and Alaska, may not be suitable in China, such as on the QTP or in northeast permafrost regions. The further experimental research will improve our knowledge for them. Based on the improved physical process or correlation, remote-sensed MAST can be integrated with this knowledge. A promising scheme is to develop an assimilation system to merge the satellite MAST with enhanced land surface model to estimate the MAGT and other thermal property of permafrost.

Additionally, to develop a quick permafrost monitoring method at regional scales, more accurate thresholds of the MAST and SFN should be identified to distinguish permafrost and seasonal frozen soil by determining the correlation of the MAST and SFN with MAGT. A temporary approach would be to transform the MODIS MAST to the MAAT based on their high correlation in permafrost mapping, using the existing MAAT threshold. However, the thermal inertia of permafrost must be considered in the monitoring of permafrost degradation, regardless of whether the MAST or the MAAT is used. Regarding the MODIS LST products, further research should focus on either the development of a MODIS cloud detection scheme that effectively recognizes completely or partially cloud-covered situations, or stronger statistical methods to estimate the true LSTs under cloudy conditions.

Acknowledgments

This study was supported by the National Natural Science Foundation of China (Grant No. 91225302, 41471359), and the Cross-disciplinary Collaborative Teams Program for Science, Technology and Innovation of the Chinese Academy of Sciences. The in situ LST data were downloaded from the Climatic Data Center, National Meteorological Information Center, China Meteorological Administration (http://cdc.cma.gov.cn/). We thank Professor Qingbai Wu for providing the modified map of permafrost distribution along the Qinghai-Tibet Highway and Railway.

References Cited

CAREERI/CAS [Cold and Arid Regions Environmental and Engineering Research Institute, and Chinese Academy of Sciences], 2006: Map of the glaciers, frozen ground and deserts in China. Beijing: SinoMaps Press, scale 1:4,000,000 (in Chinese).

Garcia, D., 2010: Robust smoothing of gridded data in one and higher dimensions with missing values. *Computational Statistics & Data Analysis*, 54: 1167–1178.

Hachem, S., Allard, M., and Duguay, C., 2009: Using the MODIS Land Surface Temperature product for mapping permafrost: an application to northern Quebec and Labrador, Canada. *Permafrost and Periglacial Processes*, 20(4): 407–416.

Hachem, S., Duguay, C. R., and Allard, M., 2012: Comparison of MODIS-derived land surface temperatures with near-surface soil and air temperature measurements in continuous permafrost terrain. *The Cryosphere*, 6: 51–69.

Haeberli, W., and Hohmann, R., 2008: Climate, glaciers and permafrost in the Swiss Alps 2050: scenarios, consequences and recommendations. *In* Kane, D. L., and Hinkel, K. M. (eds.), *Proceedings, Ninth International Conference on Permafrost*, Vol. 1. Fairbanks, Alaska: Institute of Northern Engineering, University of Alaska Fairbanks, 607–612.

Jin, H. J., Li, S. X., Cheng, G. D., Wang, S. L., and Li, X., 2000: Permafrost and climatic change in China. *Global and Planetary Change*, 26(4): 387–404.

Jin, H. J., Yu, Q. H., Lü, L. Z., Guo, D. X., He, R. X., Yu, S. P., Sun, G. Y., and Li, Y. W., 2007: Degradation of permafrost in the Xing'anling Mountains, northeastern China. *Permafrost and Periglacial Processes*, 18: 245–258.

Jin, H. J., He, R. X., Cheng, G. D., Wu, Q. B., Wang, S. L., Lü, L. Z., and Chang, X. L., 2009: Changes in frozen ground in the Source Area of the Yellow River (SAYR) on the Qinghai-Tibet Plateau, China, and their eco-environmental impacts. *Environmental Research Letters*, 4: 045206, doi http://dx.doi.org/10.1088/1748-9326/4/4/045206.

Jin, H. J., Luo, D. L., Wang, S. L., Lü, L. Z., and Wu, J. C., 2011: Spatiotemporal variability of permafrost degradation on the Qinghai-Tibet Plateau. *Sciences in Cold and Arid Regions*, 3(4): 281–305.

Jin, M. L., 2000: Interpolation of surface radiative temperature measured from polar orbiting satellites to a diurnal cycle 2. Cloudy-pixel treatment. *Journal of Geophysical Research-Atmospheres,* 105(D3): 4061–4076.

Kogan, F., Powell, A., and Fedorov, O., 2010: *Use of Satellite and In-Situ Data to Improve Sustainability.* Dordrecht, Netherlands: Springer, 362 pp.

Langer, M., Westermann, S., and Boike, J., 2010: Spatial and temporal variations of summer surface temperatures of wet polygonal tundra in Siberia—implications for MODIS LST based permafrost monitoring. *Remote Sensing of Environment*, 114(9): 2059–2069.

LIGG/CAS [Lanzhou Institute of Glaciology and Geocryology, and Chinese Academy of Sciences], 1988: Map of snow, ice and frozen ground in China. Beijing: Cartographic Publishing House, scale 1: 4,000,000.

Li, S. D., and Cheng, G. D., 1996: Map of permafrost on the Qinghai-Tibet Plateau. Lanzhou: Gansu Culture Press, scale 1:3,000,000 (in Chinese).

Li, S. X., Cheng, G. D., and Guo, D. X., 1996: Numerical simulation on the changes of permafrost on the Qinghai-Tibet Plateau under a persisting warming climate. *Science in China, Series D: Earth Sciences*, 26(4): 342–347.

Li, X., Cheng, G. D., Jin, H. J., Kang, E. S., Che, T., Jin, R., Wu, L. Z., Nan, Z. T., Wang, J., and Shen, Y. P., 2008: Cryospheric change in China. *Global and Planetary Change*, 62(3–4): 210–218.

Li, X., Li, X. W., Li, Z. Y., and 20 others, 2009: Watershed Allied Telemetry Experimental Research. *Journal of Geophysical Research*, 114: D22103, http://dx.doi.org/10.1029/2008JD011590.

Liu, X. D., Yin, Z. Y., Shao, X. M., and Qin, N. S., 2006: Temporal trends and variability of daily maximum and minimum, extreme temperature events, and growing season length over the eastern and central Tibetan Plateau during 1961–2003. *Journal of Geophysical Research*, 111: D19109, doi http://dx.doi.org/10.1029/2005JD006915.

Nan, Z. T., Huang, P. P., and Zhao, L., 2013: Permafrost distribution modeling and depth estimation in the Western Qinghai-Tibet Plateau. *Acta Geographica Sinica*, 68(3): 318–327 (in Chinese, with English abstract).

Nelson, F. E., and Outcalt, S. I., 1987: A computational method for prediction and regionalization of permafrost. *Arctic and Alpine Research*, 193: 279–288.

Ran, Y. H., Li, X., Cheng, G. D., Zhang, T. J., Wu, Q. B., Jin, H. J., and Jin, R., 2012a: Distribution of permafrost in China—An overview of existing permafrost maps. *Permafrost and Periglacial Processes,* 23: 322–333.

Ran, Y. H., Li, X., and Jin, R., 2012b: Estimation of the mean annual surface temperature and surface frost number using the MODIS land surface temperature products for mapping permafrost in China. *In* Proceedings, Tenth International Conference on Permafrost (TICOP), Salekhard, Yamal-nenets Autonomous District, Russia, 25–29 June 2012, 317–321.

Romanovsky, V. E., and Osterkamp, T. E., 1997: Thawing of the active layer on the coastal plain of the Alaskan Arctic. *Permafrost and Periglacial Processes,* 8(1): 1–22.

Sazonova, T. S., and Romanovsky, V. E., 2003: A model for regional-scale estimation of temporal and spatial variability of the active layer thickness and mean annual ground temperatures. *Permafrost and Periglacial Processes*, 14: 125–139.

Tong, B. L., Li, S. D., Pu, J. Y., and Qiu, G. Q., 1983: Principle and method of compilation of map of the distribution of permafrost along the Qinghai-Tibetan Highway (1:600,000). *In* Lanzhou Institute of Glaciology and Geocryology, Chinese Academy of Sciences (ed.), *Proceedings of the 2nd Chinese Conference on Glaciology and Geocryology*. Lanzhou: Gansu People's Press, 52–57 (in Chinese).

Wan, Z., 2008: New refinements and validation of the MODIS land-surface temperature/emissivity products. *Remote Sensing of Environment*, 112(1): 59–74.

Wang, G., Garcia, D., Liu, Y., de Jeu, R., and Dolman, A. J., 2012: A three dimensional gap filling method for large geophysical datasets: application to global satellite soil moisture observations. *Environmental Modelling & Software*, 30: 139–142.

Wang, J. C., Wang, S. L., and Qiu, G. Q., 1979: Permafrost along the Qinghai-Xizang highway. *Acta Geographica Sinica*, 34(1): 18–32 (in Chinese).

Wang, S. L., Jin, H. J., Li, S. X., and Zhao, L., 2000: Permafrost degradation on the Qinghai-Xizang (Tibet) Plateau and its environmental impacts. *Permafrost and Periglacial Processes*, 11: 43–53.

Wang, Z. X., Nan, Z. T., and Zhao, L., 2011: The applicability of MODIS land surface temperature products to simulating the permafrost distribution over Tibetan Plateau. *Journal of Glaciology and Geocryology*, 33(1): 132–143 (in Chinese, with English abstract).

Westermann, S., Langer, M., and Boike, J., 2011: Spatial and temporal variations of summer surface temperatures of high-arctic tundra on Svalbard - implications for MODIS LST based permafrost monitoring. *Remote Sensing of Environment*, 115: 908–922.

Wu, Q. B., and Liu, Y. Z., 2004: Ground temperature monitoring and its recent change in Qinghai Tibet Plateau. *Cold Regions Science and Technology*, 38: 85–92.

Wu, Q. B., Zhu, Y. L., and Liu, Y. Z., 2002: Evaluation model of permafrost thermal stability and thawing sensibility under engineering activity. *Cold Regions Science and Technology*, 34(1): 19–30.

Zhang, T., 2005: Influence of the seasonal snow cover on the ground thermal regime: an overview. *Reviews of Geophysics*, 43: RG4002, doi http://dx.doi.org/10.1029/2004RG000157.

Zhou, Y. W., Guo, D. X., Qiu, G. Q., Cheng, G. D., and Li, S. D., 2000: *Geocryology in China*. Beijing : Science Press (in Chinese).

MS accepted October 2014